CBCT images are required. Since simple double gating yields severe sparseness artifacts we propose a 5D motion compensation (MoCo) algorithm dedicated to cardio-respiratory CBCT in IGRT.

Material and Methods: Clinical patient data acquired with the TrueBeam™ CBCT system (Varian Medical Systems, Palo Alto, CA) have been used for our study. For the intrinsic respiratory and cardiac motion signal detection, about hundred overlapping regions of interests are automatically evaluated in projection space, thus yielding a robust approach independent on the anatomy shown in the projection images. In addition to respiratory gating (4D CBCT) cardiac gating is applied to obtain initial volumes. We compensate respiratory and cardiac motion in a two-step procedure. First, respiratory motion is estimated and compensated using respiratory phase binning only. Then, cardiac motion estimation is performed using respiratory-compensated images with cardiac gating. The motion estimation algorithm is based on a deformable intensity-based 3D-3D image registration method. Combining the obtained motion vector fields for respiratory and cardiac motion allows us to compensate motion for any arbitrary respiratory and cardiac target phases.

Results: Either 5D double-gated or respiratory-compensated plus cardiac-gated images both contain strong streak artifacts and high noise levels. Our 5D MoCo algorithm is able to significantly improve the image quality while maintaining the same high temporal resolution for respiratory and cardiac motion as achieved with simple double gating. Because all sparse projection streak artifacts are removed, small structures can be delineated even in areas where motion is high. The noise level of patient data is the same as that of 3D CBCT due to making use of 100 % of the projection data for each reconstructed frame.

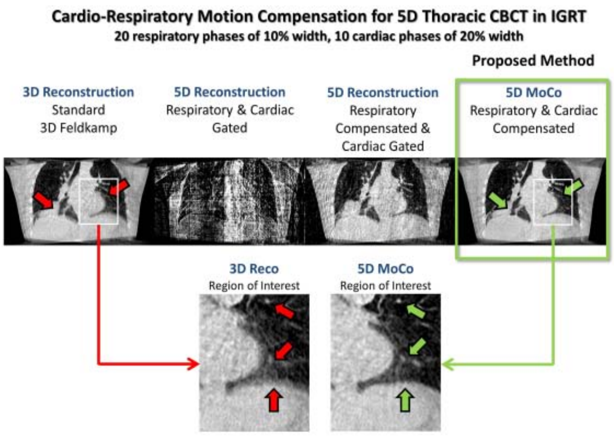

For all images a window level of -250 HU and a window width of 1400 HU was applied.

Conclusion: This work presents a reconstruction method for true 5D imaging in IGRT. Our patient data demonstrate that good image quality is achievable at identical x-ray dose levels and at acquisition times as for today's 3D CBCT. Treatments of regions close to the heart should be able to benefit from our approach.

PO-0935

Correcting diffusion weighted MR images for signal pile-up and distortions near gas pockets

L.D. Van Buuren[1], D. Polders[1], M. Milder[1], F.J. Pos[1], S.W. Heijmink[1], B. Van Triest[1], U.A. Van der Heide[1]
[1]*The Netherlands Cancer Institute, Department of Radiation Oncology, Amsterdam, The Netherlands*

Purpose or Objective: Diffusion weighted (DW) MRI is used in RT to improve tumor delineation and monitor treatment response. To minimize scan time, echo-planar imaging (EPI) is employed, but variations in the magnetic field (B0) distort EPI images due to a low pixel bandwidth in the phase-encoding (PE) direction. Geometric distortions can be corrected using a measured B0 map or by combining EPI images obtained with opposite gradients (ref. 1). However, near gas pockets B0 varies strongly. Here signal pile-up can occur, when signals from distinct, possibly non-neighboring, voxel locations are reconstructed into the same voxel. Our objective is to fully correct DW-EPI images using a combination of the above methods.

Material and Methods: On a 3T MRI (Philips Achieva), we acquired EPI images with opposite PE gradients and a dual gradient echo sequence to map B0. Both EPI images are corrected for geometric distortions by the standard correction method using the B0 map. For the new correction method, the B0 map also identifies voxels containing signal pile-up. The distortion-corrected images are averaged into a single image rejecting voxels with signal pile-up. These voxels contain data from only one EPI image. We demonstrated the correction method in a water phantom including an air cavity. The PE gradients had band widths ranging from 6 to 17 Hz/mm, comparable to clinical protocols. The corrected image was compared to raw EPI images and images corrected with the standard method. In a region-of-interest containing only pure water and signal pile-up, improvement was quantified as signal homogeneity using the coefficient of variation (CoV defined as standard deviation divided by signal mean). We applied the same method in two patients (prostate and rectal cancer), who underwent an MRI exam before radiotherapy and compared the raw images with the results of the standard correction and our full correction.

Results: With the standard correction method, distortions and intensity variations were removed in the EPI phantom images, but signal pile-up and signal loss were still visible. These were strongly reduced in our method, which was confirmed by the change in CoV in regions with signal pile-up. Here, the coefficient was 0.34 and 0.35 for the raw EPI image and B0 corrected image, respectively, and decreased to 0.12 after applying the proposed correction. Patient data are shown in the figure below. Here, rectal gas was present causing distortions and clear signal pile-up in the EPI images. After applying the correction, the signal pile-up was removed resulting in improved images.

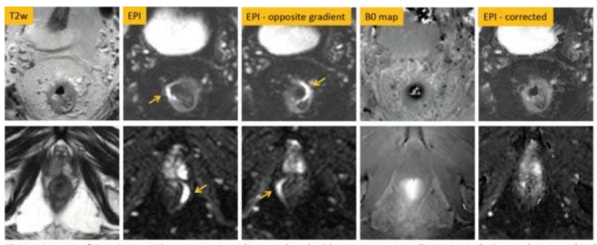

Figure: Images of 2 patients with rectum cancer (top row) and with prostate cancer (bottom row). Gas pockets are clearly visible on the high-resolution T2w images and cause variations in B0. Resulting signal pile-up in the EPI images is indicated by arrows. The black regions on the corrected EPI images result from an amplitude threshold on the B0 signal to mask out regions where B0 is unknown.

Conclusion: Our method has shown improvements in correcting EPI images, both in phantom and clinical data. It does not only correct for geometric distortions, but also for possible signal pile-up near gas pockets. Corrected DW-EPI images can improve tumor delineation and response monitoring near these regions.

Ref 1: Jezzard, P., NeuroImage 62 (2012), 648–651

PO-0936

Evolved Grow-cut: A PET based segmentation algorithm for heterogeneous tumors

H.M.T. Thevarthundiyil[1], D. Devakumar[2], Danie Kingslin Heck[2], Sasidharan Balu Krishna[3], I. Rabi Raja Singh[3], Regi Oommen[2], E. James Jebaseelan Samuel[1]
[1]*VIT University, Photonics Nuclear and Medical Physics Division School of Advanced Sciences, Vellore, India*
[2]*Christian Medical College, Department of Nuclear Medicine, Vellore, India*

[3]Christian Medical College, Department of Radiation Oncology, Vellore, India

Purpose or Objective: The purpose of the study was to evaluate the consistency, accuracy and timesaving of a grow-cut segmentation algorithm for heterogeneous tumor volumes.

Material and Methods: We present a new PET segmentation method, which is developed as a combination algorithm of Otsu and the Grow-cut segmentation algorithms and henceforth referred to as Otsu_GC. An initial contour of the tumor was defined using Otsu algorithm, which sets the threshold to minimize the intra-class variance of the tumor and its background. A concentric 3D shell was defined around the initial tumor contour at a distance of twice the slice thickness and extends up to four times the slice thickness. The space between the initial tumor contour and the inner edge of the shell ensured that the background voxels did not include the spill over voxels. The segmentation then employs the Grow-cut algorithm with the initial tumor contour and the 3D shell as the foreground and background seed respectively. The images underwent preprocessing, which included resampling to thinner slices with smaller in-plane voxel sizes that equal the CT slices. Edge preservation and contrast enhancement was achieved by convolution of high boost filter kernel in spatial domain and denoising with Gaussian blur (σ = 1pixel) filter. The implementation of preprocessing was in MATLAB and the segmentation was with SlicerRT and Grow-cut modules from 3D Slicer. The algorithm was tested on 11 heterogeneous NSCLC tumors (coefficient of variance: mean 0.35 ± 0.04) from 9 retrospective patient data. The manual contour of the PET uptake by the treating clinician was used as the ground truth for validation using Dice Similarity coefficient (DSC) and absolute volume difference as the evaluation metrics. The true contours were also compared to adaptive threshold (T*adaptive*) and 40% SUVmax threshold (T*40*) based isocontours. The PET(*Otsu-GC)* contours were also provided as the initial contour that was edited for final gross tumor volume (GTV) definition, which included composite information from CT and PET. The time taken for manual GTV contouring versus the time to edit the PET(*Otsu-GC)* contours was assessed as a measure of efficiency in this approach.

Results: Otsu_GC segmentation produced consistent contours, which were comparable to those delineated by the clinician (DSC: mean+ Std: 0.82 ± 0.062); while T*adaptive* performed reasonably well (0.80 ± 0.137) and T*40* fared poorly (0.61 ± 0.197). Compared with manual volumes Otsu-_GC volumes showed an overall overestimation (mean+ Std: 2.05 ± 4.51 cc); volumes with T*adaptive* had slight underestimation (-1.17 ± 7.33 cc) and large underestimated volumes were seen with T*40* (mean -14.49 ± 13.42 cc). The mean time of 5.72 minutes for manual GTV definition was reduced to 2.8 minutes (35%) with Otsu_GC.

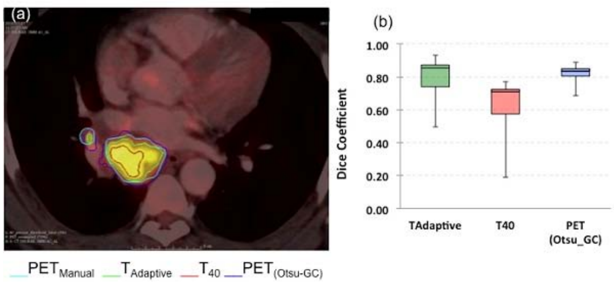

Conclusion: The proposed cellular automata based algorithm show promising results, robust enough to handle complex shaped tumor volumes with inhomogeneous tracer uptake.

PO-0937

Sound speed reconstruction in full wave ultrasound computer tomography for breast cancer detection

M. Perez-Liva[1], J.L. Herraiz[1], E. Miller[2], B.T. Cox[3], B.E. Treeby[3], J.M. Udías[1]

[1]Universidad Complutense de Madrid, Física Atómica-Molecular y Nuclear, Madrid, Spain
[2]Tufts University, Electrical & Computer Engineering, Medford- MA, USA
[3]University College London, Medical Physics and Biomedical Engineering, London, United Kingdom

Purpose or Objective: Ultrasound computer tomography (USCT) is an emerging medical imaging modality in which the acoustical properties of the tissues in the body are studied. Among these properties, the speed of sound has a close correlation with the tissue density [1], providing similar structural information to X-ray mammograms. Therefore, the sound speed maps could be employed to detect breast tumors, avoiding the use of compression and radiation. The potential of these systems as a main diagnostic tool is currently limited by the large computational cost required for image reconstruction, especially when full-wave inversion (FWI), the method that provides the best image quality, is employed [2]. In this work, we present a code based in FWI to reconstruct sound speed maps for USCT.

Material and Methods: The implemented code is based on the Adjoint Method [3] which allows finding the expression of the functional gradient of the global error norm between experimental and simulated data (Eq 1):

$$\nabla_F \varepsilon(r) = \frac{1}{{c_o}^2}\int_0^T \frac{\partial p(r,t)}{\partial t}\frac{\partial p^*(r,t)}{\partial t}dt \qquad (1)$$

$$n(r) = n^j(r) - \alpha_j \nabla_F \varepsilon^j(r) \qquad (2)$$

Here p and p* are the direct and adjoint pressure fields respectively. The functional gradient of the error is used to update the speed of sound distribution Eq 2.
The code was implemented in c++ and a CUDA version of the software k-wave [4] was employed to perform the forward and backward wave propagation. Noisy simulated data were employed to test the algorithm (Fig 1D). A reconstruction with bent-rays was used as initial guess. The simulated setup was a circular ring of detectors of 256 point elements with a field of view of 128 mm and 500 kHz of central frequency. A 2-dimensional numerical phantom representing a coronal slice of breast with 4 different tissues (fat, fibroglandular tissue, benign and malignant tumors) was studied.

Results: The reconstruction took around 9 minutes using 2 iterations with 15 subsets in an Intel Xeon 16-CPU @2.4GHz with Nvidia GEForce GTX 660. We obtained adequate recovery of the shape and values of the several structures included in the phantom and very good quality parameters in general.

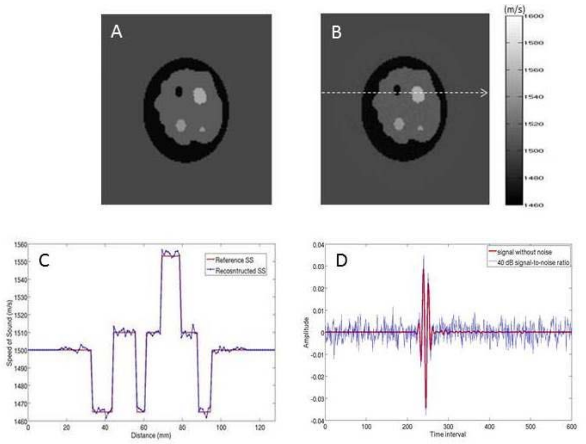

Fig. 1 A) Actual numerical breast phantom. B) Reconstructed image C) Profiles comparison D) Example of noisy reference signal.